Energy Technology
Generation, Conversion, Storage, Distribution
www.entechnol.de

Lithium Difluoro(Oxalate)Borate-Induced Interphase for High-Voltage $LiFe_{0.15}Co_{0.85}PO_4$@C Cathode by Solid-State Synthesis

Sreekumar Sreedeep, Subramanian Natarajan, Yun-Sung Lee, and Vanchiappan Aravindan**

Herein, the effect of lithium difluoro(oxalate)borate (LiDFOB) as an electrolyte additive on the electrochemical performance of $LiFe_{0.15}Co_{0.85}PO_4$@C (LFCP@C) cathode, synthesized by a scalable solid-state synthesis method is reported. Galvanostatic studies revealed better electrochemical performance among the LFCP@C (LiDFOB: 0.5–2 wt%) in a half-cell assembly compared to the $LiFe_{0.15}Co_{0.85}PO_4$ in the absence of LiDFOB. Also, among the various concentrations of LiDFOB, the LFCP@C (LiDFOB—1.5 wt%) and LFCP@C (LiDFOB—2 wt%) are optimized as suitable candidates for further electrochemical studies owing to the high discharge capacities of 116 and 118 mAh g^{-1}. In addition, the electrochemical impedance studies (EIS) exhibited an increase in the charge–transfer resistance (R_{ct}) as the amount of LiDFOB was increased, whereas a lower R_{ct} value is observed in the absence of additive. In addition, the diffusion coefficient calculation is calculated using the EIS data, which shows a diffusion coefficient in the order of $\approx 10^{-13}$ cm^2 s^{-1}. However, as the amount of LiDFOB is increased from 0 to 2 wt%, a decrease in the diffusion coefficient is observed owing to the formation of a stable and thicker passivation layer.

1. Introduction

The rapid climatic changes caused due to global warming and the overexploitation of fossil fuels are the major threats the modern world is facing. The transition from primitive energy sources such as coal and petroleum to eco-friendly and sustainable energy technology is necessary to deal with these adverse conditions.[1–3] Thus, the development of energy storage devices is gaining a lot of importance. Among the various energy storage devices developed so far, lithium-ion batteries (LIBs) hold a superior position compared to other conventional technologies. The properties such as high energy density, high power density, and low safety limits possessed by LIBs have made it applied in a wide range of applications, including portable electronic devices and emission-free electric vehicles (EVs).[3–7] Thus, to cope with these current energy demands, enhancing the energy density of LIBs is much more important. Among the different components of LIB, the cathode active material plays a crucial role in enhancing the energy density.[5,8,9]

Conventional cathodes such as $LiCoO_2$, due to various setbacks such as high cost, safety concerns, and low redox potential, had motivated the search for an alternate cathode. The olivine-structured $LiMPO_4$ (M: Mn, Fe, Co, and Ni), owing to its excellent thermal stability, high specific capacity, and high energy density, has emerged as a promising cathode for LIBs.[8–10] Even though the commercialization of $LiFePO_4$ has been achieved, the low redox potential of the $Fe^{3+/2+}$ couple (3.4 V vs Li) results in a low (theoretical) energy density (580 Wh kg^{-1}) compared to other members of this class.[11,12] These setbacks of $LiFePO_4$ had extended the research to other members of the olivine class, especially $LiCoPO_4$ (LCP), owing to its high redox potential of the $Co^{3+/2+}$ couple (4.8 V vs Li), the high theoretical energy density of 800 Wh kg^{-1}, and excellent thermal stability due to strong P—O covalent bond.[10] Although possessing all the characteristics of an excellent cathode, the development of $LiCoPO_4$ has been hindered by the low electronic as well as Li^+ ion conductivity and low coulombic efficiency. In addition, the decomposition of electrolytes at high potential will also cause a fast capacity fading, which results in low cycle stability.[8]

Of the various strategies that have been employed so far, the methods such as carbon coating,[13] metal-ion doping,[14–17] and electrolyte optimization[9,18–25] are found to be more promising. Carbon coating primarily focuses on enhancing electronic conductivity and also improves discharge capacities. In addition, the layer of carbon will prevent the contact of the electrolyte with lattice, hence mitigating the unsatisfactory side reaction. However, as the amount of added carbon is increased beyond a certain limit, a higher value of electronic conductivity is still observed, whereas it will block the reversible transfer of Li^+ ion from $LiCoPO_4$, hence reducing the Li^+ ion conductivity.[26]

S. Sreedeep, S. Natarajan, V. Aravindan
Department of Chemistry
Indian Institute of Science Education and Research (IISER)
Tirupati 517507, India
E-mail: aravindan@iisertirupati.ac.in

Y.-S. Lee
School of Chemical Engineering
Chonnam National University
Gwang-ju 61186, Republic of Korea
E-mail: leeys@chonnam.ac.kr

The ORCID identification number(s) for the author(s) of this article can be found under https://doi.org/10.1002/ente.202200988.

DOI: 10.1002/ente.202200988

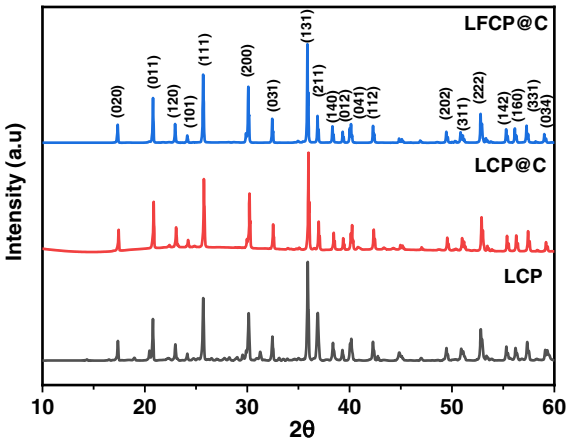

Figure 1. XRD pattern of $LiFe_{0.15}Co_{0.85}PO_4$@C (LFCP@C), $LiCoPO_4$@C (LCP@C), and $LiCoPO_4$ (LCP).

Metal-ion doping, mainly Fe doping, aims at improving the bulk Li^+ ion conductivity in $LiCoPO_4$. Kang et al.[27] had shown using various ab initio calculations and absorption spectroscopy studies that the preferential occupation of Fe in the 4c site of Co will suppress the antisite mixing of Li and Co in the 4a and 4c sites, hence improving the cycle stability of $LiCoPO_4$.

The optimization of electrolytes using additives is another plausible approach that can be employed to improve the cycle stability as well as the electrochemical performance of $LiCoPO_4$. The preferential decomposition of the additives prior to the electrolytes results in the formation of a protective film/passivation layer over the cathode, thereby suppressing the decomposition of electrolytes at a higher potential and preventing the lattice from the parasitic side reactions of the electrolyte, hence mitigating the issue of low cycle stability in $LiCoPO_4$.[9,21]

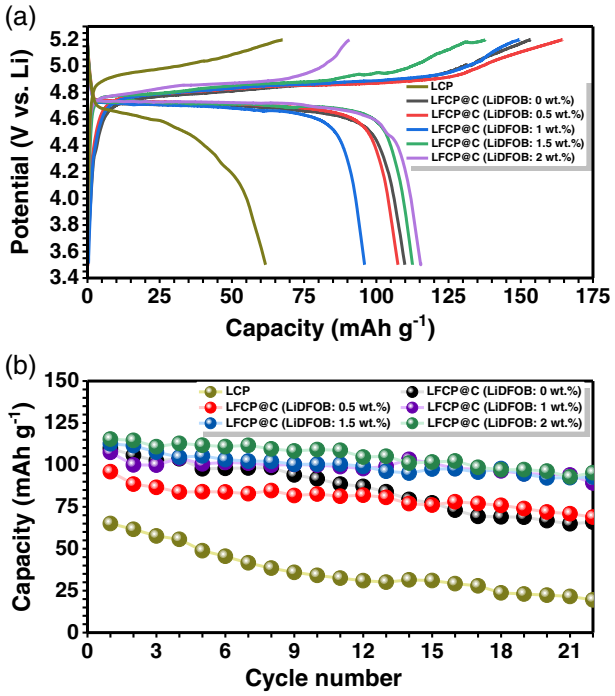

Figure 3. a) Charge–discharge curve and b) capacity versus cycle number plots of $LiFe_{0.15}Co_{0.85}PO_4$@C (LFCP@C) (LiDFOB: 2 wt%) at a current density of 10 mA g^{-1}.

Among the various additives that have been used so far, the use of boron-based additives are gaining lots of attention. Lithium difluoro(oxalate)borate (LiDFOB), owing to the formation of a stable solid electrolyte interphase (SEI), can be used as a suitable electrolyte additive for $LiCoPO_4$.[19] Meng et al.[19] showed that the usage of LiDFOB as an additive in normal carbonate electrolytes

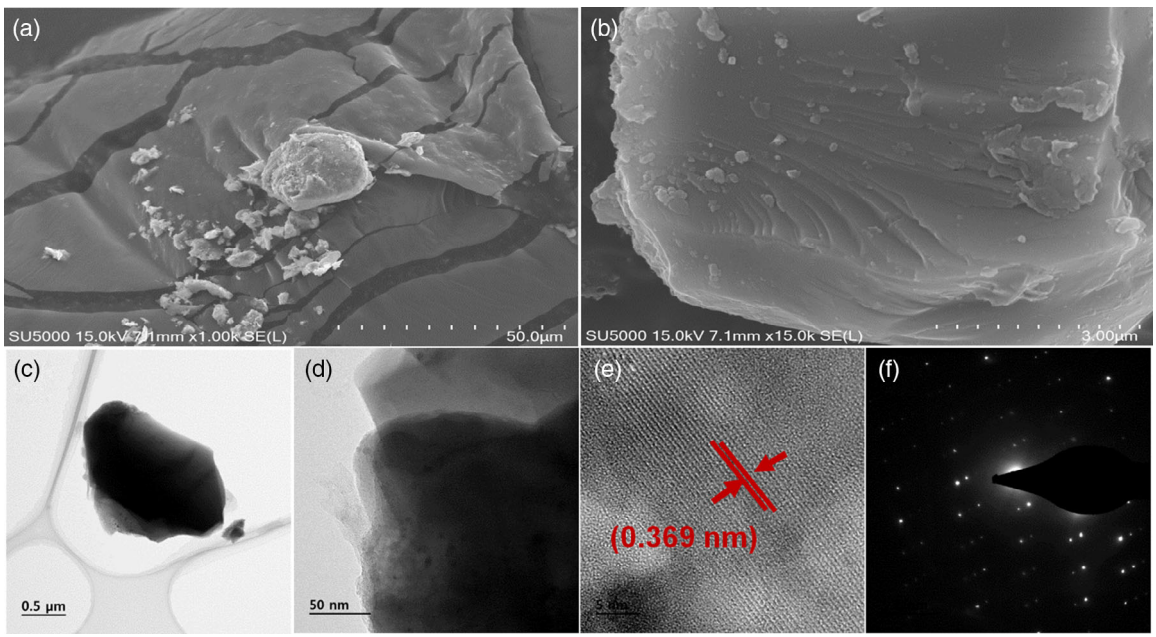

Figure 2. a,b) FE-SEM images of $LiFe_{0.15}Co_{0.85}PO_4$@C (LFCP@C), and c–f) HR-TEM images of $LiFe_{0.15}Co_{0.85}PO_4$@C (LFCP@C).

had improved the initial discharge capacity to 138 mAh g^{-1} with a capacity retention of 69.4% after 40 cycles. In addition, the high solubility of LiDFOB in carbonate electrolytes has made it more attractive compared to other boron additives such as Lithium bis(oxalato)borate.[20]

Taking into consideration the various challenges associated with $LiCoPO_4$, here we are attempting to mitigate these setbacks by combining the strategies of Fe doping along with electrolyte optimization using LiDFOB as an additive. A scalable solid-state approach has been employed for the synthesis of Fe-doped $LiCoPO_4$@C, i.e., $LiFe_{0.15}Co_{0.85}PO_4$@C (LFCP@C), and the effect of different concentrations of LiDFOB on the electrochemical performance of $LiFe_{0.15}Co_{0.85}PO_4$ has been investigated. In addition, other studies such as electrochemical impedance studies (EIS), in situ EIS, and diffusion coefficient studies have been carried out to prove the formation of a stable and thicker SEI layer due to the decomposition of LiDFOB.

2. Results and Discussion

The structural features of LFCP@C have been analyzed using a powder X-ray diffraction (XRD). The XRD (**Figure 1**) pattern of the as-synthesized LFCP@C is in agreement with pristine LCP, thereby crystallizing in an orthorhombic lattice with a Pnma space group (ICDD No: 89-6192).[10,13] The unit cell parameters have been calculated as $a = 10.22$ Å, $b = 5.93$ Å, and $c = 4.69$ Å. Also, the unit cell volume has been calculated from the refined parameters as 284.94 $Å^3$. In addition, the prominent diffraction peaks at 2θ values of 22.1, 26.5, 32, and 36.2 denote the planes (210), (020), (220), and (002), respectively. However, no characteristic peaks corresponding to Fe and carbon are not observed in the spectra owing to their low content in the sample, and there is secondary phase appeared. The Raman spectra (Figure S1, Supporting Information) of LFCP@C exhibit peaks at 1,352 and 1,603 cm^{-1}, corresponding to the D-band or the defective band and G-band or the graphitic carbon. In addition, the degree of disorderliness denoted by I_D/I_G has been calculated to be 0.97, which indicates that the majority of carbon is present in the crystalline state.[28]

The field-emission scaaning electron microscopy (FE-SEM) image (**Figure 2**a,b) of LFCP@C depicts a nonuniform size distribution among the particles, which occurs due to particle agglomeration during carbon coating. The transmission electron microscopy (TEM) image (Figure 2c–f) depicts the presence of a semiuniform carbon coating on the surface of LFCP@C.

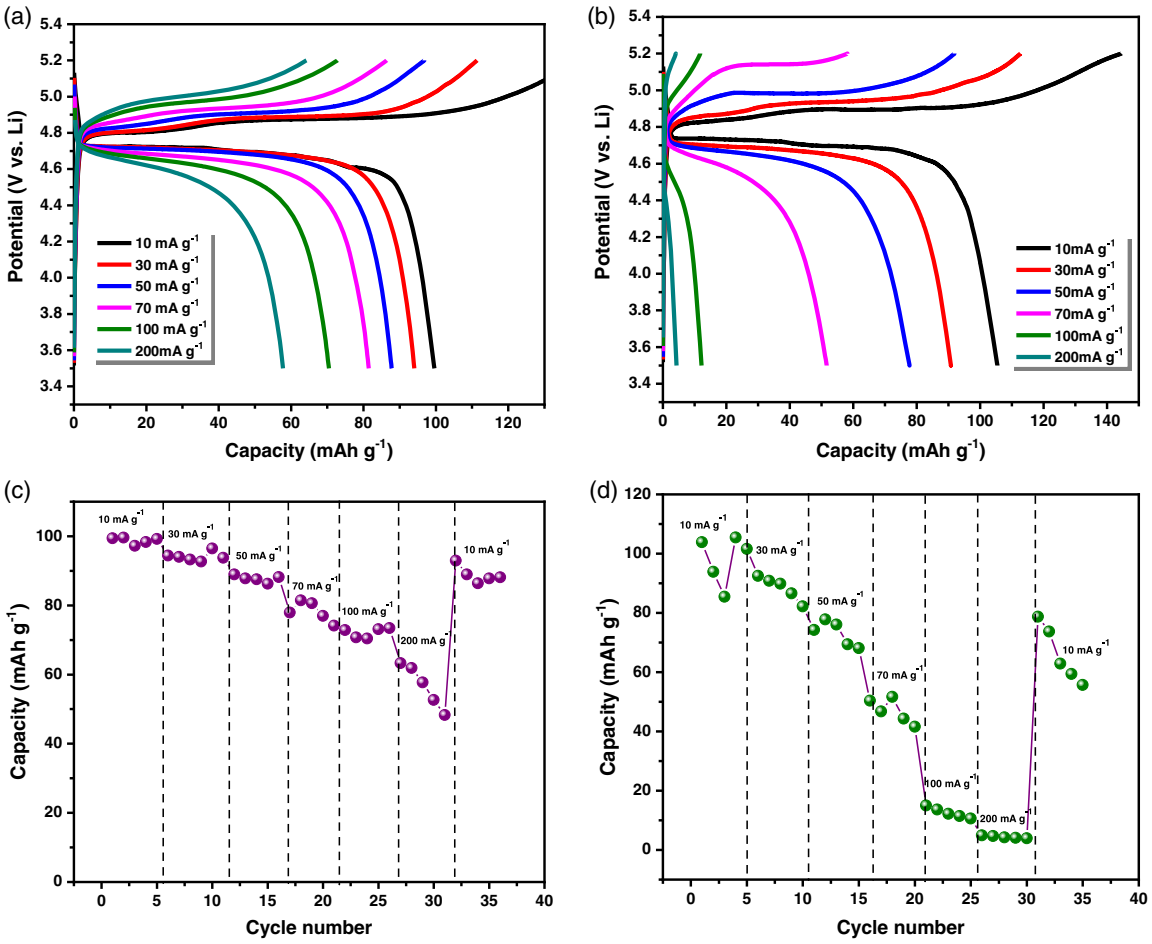

Figure 4. Rate performance of a,c) LFCP@C (LiDFOB: 1.5 wt%), and b,d) LFCP@C (LiDFOB: 2 wt%) at current densities of 10, 30, 50, 70, 100, and 200 mA g^{-1}.

In addition, the fringe width has been calculated from the TEM image (Figure 2e) as 0.369 nm, which corresponds to the (011) crystal plane. The selected area electron diffraction (SAED) pattern (Figure 2f) further illustrates the formation of a crystalline compound.

The electrochemical performance of LFCP@C at different LiDFOB concentrations ranging from 0 to 2 wt% has been done at a current density of 10 mA g^{-1} within a potential window of 3.5–5.2 V versus Li. The galvanostatic charge–discharge (GCD) curves (**Figure 3**a) clearly illustrate the enhancement in the electrochemical performance of LFCP@C upon the usage of LiDFOB as an additive. This improvement in the electrochemical performance of LFCP@C has been attributed to the formation of a stable and robust SEI layer, thereby mitigating the irreversible capacity loss and preventing the decomposition of electrolytes at higher potential.[18,21,29–31] Also, from the cycling profile, the LFCP@C (LiDFOB—1.5 wt%) and LFCP@C (LiDFOB—2 wt%) exhibit excellent discharge capacities of 113 and 116 mAh g^{-1} with a capacity retention of 79% and 81% after 23 cycles (Figure 3b). However, a gradual capacity fading is observed from the 24th cycle, which can be due to electrolyte decomposition since the half-cells studied in a high elevated potential range with a lower current rate. Adding to this, the rate performance (**Figure 4**a–d, S2, Supporting Information) exhibits better capacity retention for the LFCP@C (LiDFOB—1.5 wt%) and LFCP@C (LiDFOB—2 wt%) at high current densities of 100 and 200 mA g^{-1} compared to other LiDFOB concentrations. Therefore, it can be concluded that the concentration of LiDFOB in the range of 1.5–2 wt% is optimum to realize the better electrochemical performance of LFCP@C. Along with it, the GCD of the as-prepared compound has been done within the temperature range of –10 to 10 °C. The cycling profile (**Figure 5**a,b) suggests that there is an enhancement in the electrochemical performance of LFCP@C (LiDFOB—2 wt%) at a higher temperature of 10 °C, whereas electrochemical performance becomes poor upon decreasing the temperature to –10 and 0 °C. The above observation makes it clear that on lowering the temperature to –10 °C, the freezing of electrolytes occurs, leading to a lowering in the mobility of Li^+ ions. In contrast, as the temperature is increased to 10 °C, there is an enhancement in the mobility of Li^+ ions, thereby resulting in a better electrochemical performance.[17]

In addition, the Nyquist plots (**Figure 6**b) of LFCP@C (LiDFOB: 0–2 wt%) show the comparison of the charge–transfer resistance (R_{ct}) for the different concentrations of LiDFOB. From the Nyquist plot, an increase in the R_{ct} value can be observed as the concentration of LiDFOB has been increased from 0 to 2 wt%, which can be accounted by the resistance offered to Li^+ ion mobility due to the formation of a stable SEI layer.[9] In addition, the in situ impedance study (**Figure 7**a–d) has been

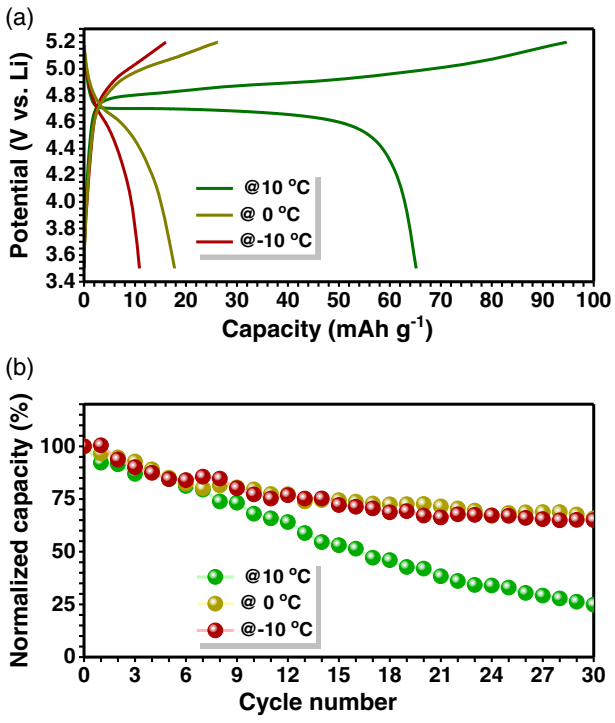

Figure 5. a) Charge–discharge and b) capacity versus cycle number plot of $LiFe_{0.15}Co_{0.85}PO_4$@C (LFCP@C) (LiDFOB: 2 wt%) at temperatures ranging from –10 to 10 °C.

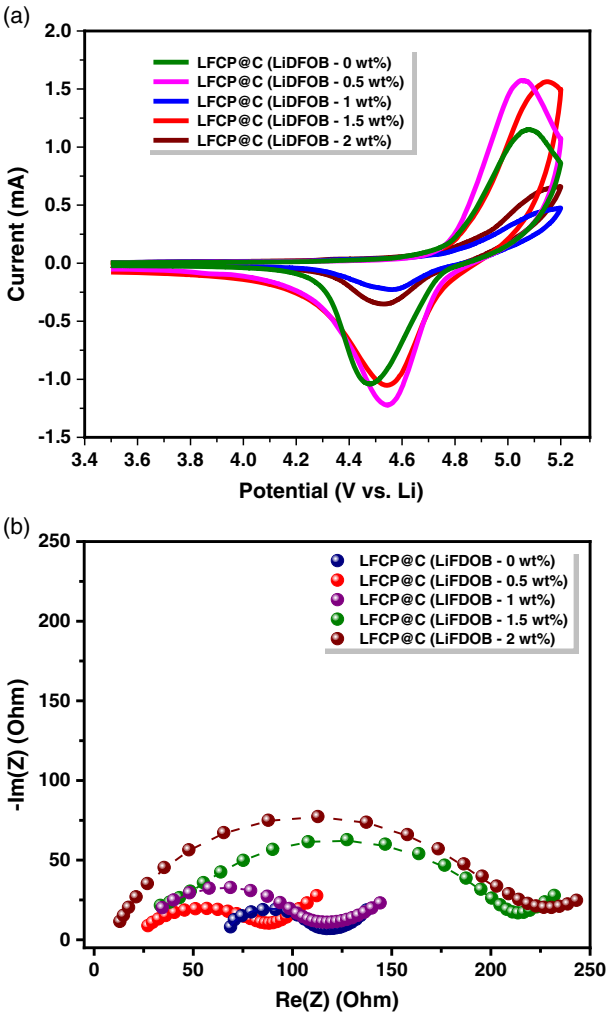

Figure 6. Plot showing a) cyclic voltammetry of LFCP@C (LiDFOB: 0–2 wt%) at a scan rate of 0.1 mV s^{-1} and b) corresponding impedance curves.

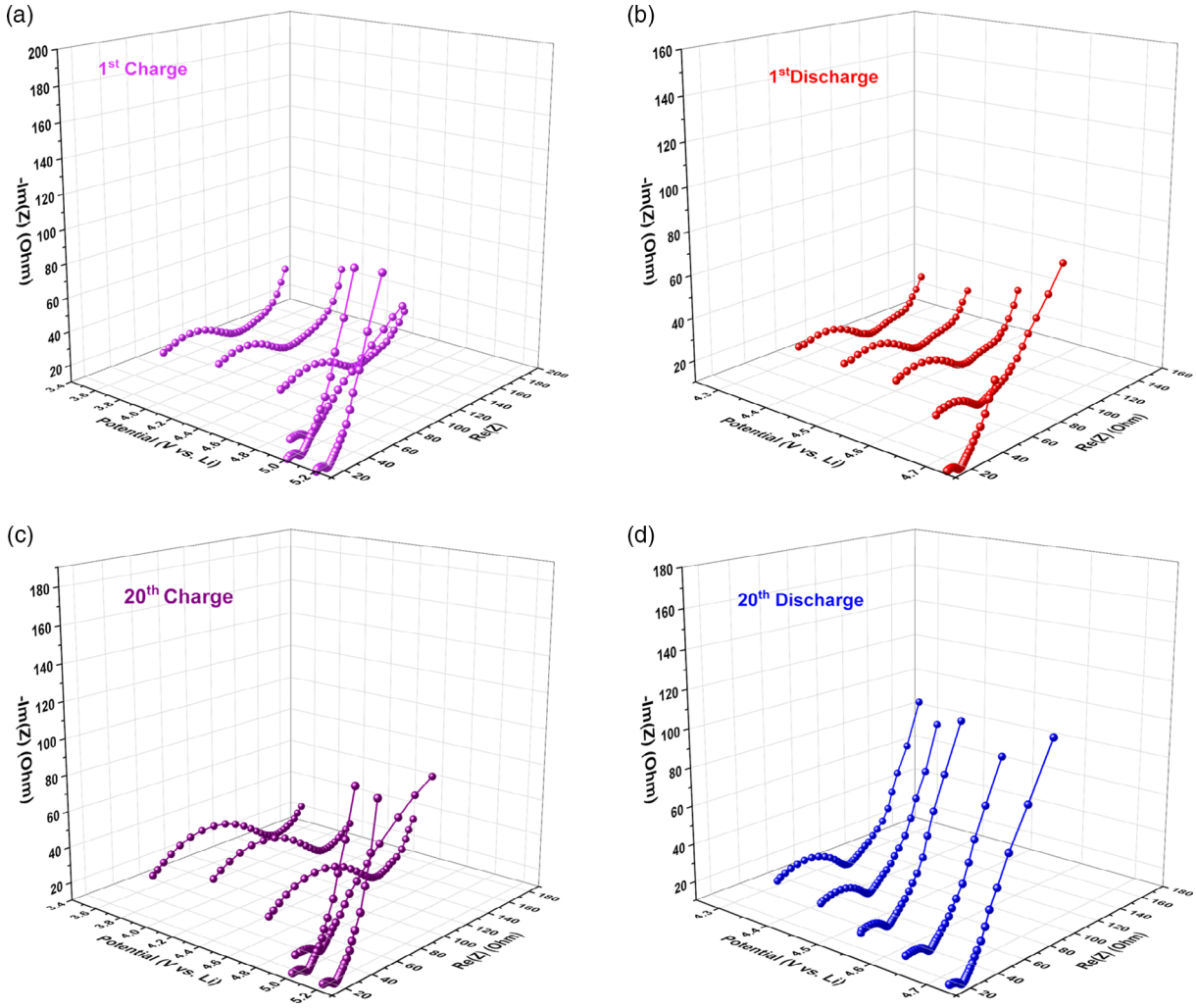

Figure 7. In situ impedance study of LFCP@C (LiDFOB: 2 wt%) corresponding to the a,b) 1st cycle c,d) 20th cycle charge–discharge. The open circuit potential (OCV) of the cell is 2.8 V.

carried out to investigate the stability of the SEI layer as the cycling progresses.[32] However, it can be observed from the Nyquist plot that as the cycling progresses from the 1st to 20th cycle, there is not much rise in the R_{ct} value, which confirms the formation of a stable SEI layer, thereby mitigating the irreversible Li^+ ion consumption.

The cyclic voltammetry (CV) (Figure 6a and S3, Supporting Information) of LFCP@C (LiDFOB: 0–2 wt%) has been carried out at a scan rate of 0.1 mV s^{-1} to determine the electrochemical reactions accompanying the redox process. From the CV, it can be observed that LFCP@C (LiDFOB: 0–2 wt%) exhibits oxidation peaks corresponding to Co^{3+}/Co^{2+} redox couple at potentials of 5.07, 5, 5.17, 5.16, and 5.18 V versus Li. But it can be observed from the CV that there is an enhancement in the polarization as the concentration of LiDFOB is increased from 0.5 to 2 wt%, whereas only slight polarization can be observed in the absence of LiDFOB, which is consistent with the GCD plot.

The apparent Li^+ ion diffusion coefficient for LFCP@C (LiDFOB: 0–2 wt%) has been determined using electrochemical impedance spectroscopy (EIS). The evaluation of the diffusion coefficient has been carried out from the low-frequency Warburg region of the Nyquist plot. Now, the diffusion coefficient is determined using the formula

$$D_{Li+} = R^2T^2//2A^2n^4F^4C^2\sigma_w{}^2 \quad (1)$$

Of which R is the universal gas constant (8.314 J K^{-1} mol^{-1}), T is the temperature, A is the electrode cross-sectional area, n is the number of Li^+ ions involved in the redox reaction, F is the Faraday constant (96 500 C mol^{-1}), C is the concentration of Li^+ ions, and σ_w is the slope obtained from the plot of real impedance and the reciprocal square root of the angular frequency, i.e., Z versus $\omega^{-1/2}$ (Figure 5 and 6, **Table 1**).[33,34] Based on the calculated values of diffusion coefficients (**Table 2**), it has been observed that the LFCP@C (LiDFOB: 0–2 wt%) exhibits diffusion coefficients in the order of $\approx 10^{-13}$ cm^2 s^{-1}. In addition, as the amount of LiDFOB has increased from 0 to 2 wt%, the value of the diffusion coefficient has decreased. This is consistent

Table 1. Impedance parameters like χ^2, *R*1, *R*2, and *R*3 values.

Additive composition	Diffusion coefficient [$cm^2 s^{-1}$]
LCP@C	1.42×10^{-14}
LCP@C	1.61×10^{-14}
LFCP@C (LiDFOB: 0 wt%)	2.42×10^{-13}
LFCP@C (LiDFOB: 0.5 wt%)	2.12×10^{-13}
LFCP@C (LiDFOB: 1 wt%)	2.01×10^{-13}
LFCP@C (LiDFOB: 1.5 wt%)	1.58×10^{-13}
LFCP@C (LiDFOB: 2 wt%)	1.15×10^{-13}

Table 2. Diffusion coefficient calculated from the impedance data for $LiFe_{0.15}Co_{0.85}PO_4$@C (LiDFOB: 0–2 wt%).

LiDFOB concentration	*R*1	*R*2	*R*3	χ^2
LiDFOB-0 wt%	4.02	36.04	1.793	4.5
LiDFOB-0.5 wt%	34.48	44	11.65	5.2
LiDFOB-1 wt%	64.95	83.42	30.09	7.9
LiDFOB-1.5 wt%	3.71	21.36	58.43	9.6
LiDFOB-2 wt%	7.968	98.96	122.2	9.5

with the fact that a stable SEI layer has been formed due to the decomposition of LiDFOB, and as the amount of LiDFOB is increased from 0 to 2 wt%, the as-formed SEI layer becomes thicker, thereby ceasing the Li^+ ion mobility, which eventually leads to a decrease in the Li^+ ion diffusion coefficient. Thus, the calculation of the diffusion coefficient further illustrates the fact that the use of LiDFOB as an additive improves the electrochemical performance of LFCP@C by the formation of a stable SEI layer compared to that of a normal electrolyte.

3. Conclusion

The development of novel electrolyte additives is gaining a lot of interest in the development of high-voltage cathodes, especially LCP. Here, we successfully illustrated the effect of LiDFOB as an additive on the electrochemical performance of LFCP@C. Among the various LiDFOB concentrations, the LFCP@C (LiDFOB: 1.5 wt%) and LFCP@C (LiDFOB: 2 wt%) have been optimized for further electrochemical studies owing to the high discharge capacities of 113 and 116 mAh g^{-1}. As expected, the Nyquist plot showed a large R_{ct} value in the case of LFCP@C (LiDFOB: 2 wt%) due to the formation of a stable SEI layer, whereas a low value of R_{ct} in the absence of LiDFOB suggests that no SEI layer was formed. Further, the in situ impedance study confirmed that a stable SEI layer had been formed owing to the fact that there is not much change in R_{ct} value between the Nyquist plot of the 1st and 20th cycle. Apart from this, the diffusion coefficient has been calculated from the Warburg region of the Nyquist plot, which had shown a lowering in the Li^+ ion mobility as the amount of LiDFOB is increased from 0 to 2 wt%. This result further confirms that a stable SEI layer has been formed, thereby providing resistance to the mobility of Li^+ ions. Hence, it proves the superior electrochemical performance of LFCP@C in the presence of LiDFOB as an additive. Thus, the research on electrolyte additives must be extended to other class, which includes phosphorus-, sulfur-, and carbonate-based additives, for achieving the commercialization of LCP.

4. Experimental Section

Synthesis: The preparation of LFCP@C was carried out by a solid-state synthesis approach on a gram scale. All the precursors, including Li_2CO_3 (Sigma-Aldrich, ≥99%), $(NH_4)_2HPO_4$ (Sigma-Aldrich, ≥98%), Co_3O_4 (Sigma-Aldrich), and $Fe(CH_3COO)_2$ (Sigma-Aldrich, ≥99.99%), were mixed properly and were heated to a temperature of 800 °C at a ramp rate of 5 °C min^{-1} in an open-air atmosphere. The obtained sample was ball-milled in a planetary ball-miller (Retsch PM200, Germany) for a period of 2 h. Further, the ball-milled sample was subjected to the carbon coating in which glucose (Sigma-Aldrich, ≥99.5%) was used as the carbon precursor. Both LFCP@C and glucose were mixed properly, and the solution was prepared in a weight ratio of 2:1. The solution was then subjected to heating to remove the water present, and the sample was obtained in a charred form. The sample was then heated in an argon atmosphere to a temperature of 800 °C at a ramp rate of 5 °C min^{-1}. At last, the sample was grounded well using a mortar and pestle into fine powder. The carbonaceous material present in the cathode is estimated to ≈10 wt% through thermogravimetric analysis (Figure S6, Supporting Information).

Preparation of Electrolyte: The electrolyte was prepared using 1 M $LiPF_6$ dissolved in ethylene carbonate (EC) and dimethyl carbonate (DMC) (1:1 weight ratio, Lipaste, Tomiyama) by varying the concentration of LiDFOB (Sigma-Aldrich) from 0 to 2 wt% inside an Ar-filled glovebox with an oxygen level <0.l ppm. None of the salt or solvent used had been subjected to any purification or pretreatment and had been used directly.

Electrochemical Characterization: The preparation of the electrode was carried out by mixing 10 mg of LFCP@C, 2 mg of conductive additive (acetylene black), and 2 mg of binder [teflonized acetylene black-2 (TAB)] in a mortar and pestle using ethanol as a solvent into a freestanding film and had been pressed on a 14 mm stainless steel mesh (Goodfellow, UK), which will act as a current collector. Now, the electrode was dried overnight in a vacuum oven at 75 °C and was made into a half-cell in an Ar-filled glove box using a glass microfiber separator (Whatman, UK) against metallic lithium as the reference electrode in a CR2016 coin cell. Now, further half-cell studies such as GCD, EIS, and CV were carried out in a battery tester (Biologic, France).

Material Characterization: The structural analysis of LFCP@C was done using XRD (Rigaku, Smart Lab 9 kW) at 0.5° min^{-1} scan rate in a monochromatic Cu-Kα radiation ($\lambda = 1.5414$ Å). The material composition of the sample has also been determined using Raman spectral analysis. The HR-TEM (TECNAI, Philips, the Netherlands, 200 keV) and FE-SEM (S-4700, Hitachi, Japan) were carried out for the morphological as well as structural analysis of the sample.

Acknowledgements

S.S. acknowledges the Council of Scientific and Industrial Research (CSIR), Govt. of India for the Fellowship. Y.S.L. acknowledges the financial support from the National Research Foundation of Korea (NRF) grant funded by the Korean government (Ministry of Science, ICT & Future Planning) (No. 2019R1-A2C1007620). V.A. acknowledges financial support from the Science and Engineering Research Board (SERB), a statutory body of the Department of Science & Technology, Govt. of India, through the Ramanujan Fellowship (SB/S2/RJN-088/2016) and Swarnajayanti Fellowship (SB/SJF/2020-21/12).

Conflict of Interest

The authors declare no conflict of interest.

Data Availability Statement

The data that support the findings of this study are available from the corresponding author upon reasonable request.

Keywords

electrolyte additives, Fe doping, high-voltage cathodes, $LiCoPO_4$, lithium-ion batteries

Received: August 24, 2022
Revised: October 11, 2022
Published online: October 26, 2022

[1] J. B. Goodenough, Y. Kim, *Chem. Mater.* **2010**, *22*, 587.
[2] D. Deng, *Energy Sci. Eng.* **2015**, *3*, 385.
[3] N. Nitta, F. Wu, J. T. Lee, G. Yushin, *Mater. Today* **2015**, *18*, 252.
[4] S. Natarajan, V. Aravindan, *Adv. Mater.* **2018**, *8*, 1802303.
[5] Y. Tian, G. Zeng, A. Rutt, T. Shi, H. Kim, J. Wang, J. Koettgen, Y. Sun, B. Ouyang, T. Chen, Z. Lun, Z. Rong, K. Persson, G. Ceder, *Chem. Rev.* **2021**, *121*, 1623.
[6] J. El Haddad, L. Canioni, B. Bousquet, *Spectrochim. Acta, Part B* **2014**, *101*, 171.
[7] S. Goriparti, E. Miele, F. De Angelis, E. Di Fabrizio, R. Proietti Zaccaria, C. Capiglia, *J. Power Sources* **2014**, *257*, 421.
[8] J. Ludwig, T. Nilges, *J. Power Sources* **2018**, *382*, 101.
[9] S. Sreedeep, S. Natarajan, V. Aravindan, *Curr. Opin. Electrochem.* **2022**, *31*, 100868.
[10] M. Zhang, N. Garcia-Araez, A. L. Hector, *J. Mater. Chem. A* **2018**, *6*, 14483.
[11] Z. Yang, Y. Dai, S. Wang, J. Yu, *J. Mater. Chem. A* **2016**, *4*, 18210.
[12] L. X. Yuan, Z-H. Wang, W.-X. Zhang, X.-L. Hu, J.-T. Chen, Y.-H. Huang, J. B. Goodenough, *Energy Environ. Sci.* **2011**, *4*, 269.
[13] S. Sreedeep, V. Aravindan, *Mater. Lett.* **2021**, *291*, 129609.
[14] S. Brutti, J. Manzi, D. Meggiolaro, F. M. Vitucci, F. Trequattrini, A. Paolone, O. Palumbo, *J. Mater. Chem. A* **2017**, *5*, 14020.
[15] D. Di Lecce, J. Manzi, F. M. Vitucci, A. De Bonis, S. Panero, S. Brutti, *Electrochim. Acta* **2015**, *185*, 17.
[16] K. J. Kreder, A. Manthiram, *ACS Energy Lett.* **2017**, *2*, 64.
[17] S. Sreedeep, S. Natarajan, Y.-S. Lee, V. Aravindan, *Electrochim. Acta* **2022**, *419*, 140367.
[18] N. Ehteshami, L. Ibing, L. Stolz, M. Winter, E. Paillard, *J. Power Sources* **2020**, *451*, 227804.
[19] M. Hu, J. Wei, L. Xing, *J. Appl. Electrochem.* **2012**, *42*, 291.
[20] V. Aravindan, J. Gnanaraj, S. Madhavi, H. K. Liu, *Chem.—Eur. J.* **2011**, *17*, 14326.
[21] L. Yang, T. Markmaitree, B. L. Lucht, *J. Power Sources* **2011**, *196*, 2251.
[22] V. Aravindan, Y. L. Cheah, W. C. Ling, S. Madhavi, *J. Electrochem. Soc.* **2016**, *159*, 1435.
[23] D. Di Lecce, J. Hassoun, *ACS Omega* **2018**, *3*, 8583.
[24] V. Marangon, L. Minnetti, M. Adami, A. Barlini, J. Hassoun, *Energy Fuels* **2021**, *35*, 10284.
[25] L. Minnetti, V. Marangon, J. Hassoun, *Adv. Sustainable Syst.* **2022**, *6*, 10292.
[26] J. Wolfenstine, J. Read, J. L. Allen, *J. Power Sources* **2007**, *163*, 1070.
[27] D. Han, Y. Kang, R. Yin, M. Song, H. Kwon, *Electrochem. Commun.* **2009**, *11*, 137.
[28] R. Sharabi, E. Markevich, V. Borgel, G. Salitra, G. Gershinsky, D. Aurbach, G. Semrau, M. A. Schmidt, N. Schall, C. Stinner, *J. Power Sources* **2012**, *203*, 109.
[29] R. Sharabi, E. Markevich, K. Fridman, G. Gershinsky, G. Salitra, D. Aurbach, G. Semrau, M. A. Schmidt, N. Schall, C. Bruenig, *Electrochem. Commun.* **2013**, *28*, 20.
[30] A. M. Haregewoin, A. S. Wotango, B. J. Hwang, *Energy Environ. Sci.* **2016**, *9*, 1955.
[31] J. Li, Z. Wang, *J. Power Sources* **2020**, *450*, 227648.
[32] K. Subramanyan, Y. S. Lee, V. Aravindan, *J. Colloid Interface Sci.* **2021**, *582*, 51.
[33] X. Wu, M. Meledina, H. Tempel, H. Kungl, J. Mayer, R.-A. Eichel, *J. Power Sources* **2020**, *450*, 227726.
[34] T. Q. Nguyen, C. Breitkopf, *J. Electrochem. Soc.* **2018**, *165*, E826.